J Nanostruct 11(4): 790-801, Autumn 2021

RESEARCH PAPER

CQDs/BiOCl Photocatalysts for the Efficient Treatment of Congo Red Aqueous Solution under Visible Light

Mohsen Padervand [1], Mojtaba Mazloum [1], Alireza Bargahi [1], Naser Arsalani [2]*

[1] *Department of Chemistry, Faculty of Science, University of Maragheh, Maragheh, Iran*

[2] *Research Laboratory of Polymer, Department of Organic and Biochemistry, Faculty of Chemistry, University of Tabriz, Tabriz, Iran*

ARTICLE INFO

Article History:
Received 17 July 2021
Accepted 24 September 2021
Published 01 October 2021

Keywords:
BiOCl
CQDs
Congo red
Photodegradation
Visible-light photocatalysis

ABSTRACT

The surface of BiOCl nanosheets, prepared by a simple hydrothermal method, was decorated by carbon quantum dots (CQDs) through a microwave-assisted procedure. According to Diffuse Reflectance spectroscopy (DRS), light-harvesting properties improved significantly, which was explainable based on the bandgap of the final photocatalyst, 1.15 eV. Elemental analysis results coupled with scanning electron microscopy (SEM) images proved changes in the morphological characteristics after adding CQDs to the support; While in powder X-ray diffraction (XRD) patterns, there was no indication of further crystalline phases on the surface of BiOCl nanosheets. The photocatalytic performance of the nanostructures was evaluated by Congo red dye removal under visible light at room temperature. The photoreaction obeyed first-order kinetics with the rate constant of 0.011 min-1. According to the experiments, photodegradation was noticeably affected by catalyst dosage, dye concentration, and pH, which were all optimized. The photocatalytic performance of the prepared nanostructure was mechanistically discussed, considering the desirable role of CQDs towards reaching superior photoactivity.

How to cite this article
Padervand M., Mazloum M., Bargahi A., Arsalani N. CQDs/BiOCl Photocatalysts for the Efficient Treatment of Congo Red Aqueous Solution under Visible Light. J Nanostruct, 2021; 11(4): 790-801. DOI: 10.22052/JNS.2021.04.016

INTRODUCTION

Photocatalytic processes are sorted as reliable methodologies to produce clean and renewable energy (through water splitting) and destroy harmful water pollutants taking advantage of cheap energy sources and affirmed productive mechanisms [1-5]. As the key point of such processes, the photogenerated reactive oxygen species ($O_2^{\cdot-}$, $OH^{\cdot}$, $HO_2^{\cdot}$), after absorbing the photons, promote various degrading kinds of organic pollutants [6-9]. TiO_2 is the most famous photocatalyst with properties, e.g., least toxicity, low cost, easy preparation, and high stability; its practical application is limited because of the large bandgap (3.2 eV) and fast electron-hole recombination [10, 11]. Compared to TiO_2-based photocatalysts, bismuth-based semiconductors such as BiOX compounds (X = Cl, Br, I) can have exhibited excellent photocatalytic performance under UV and visible light irradiation [12, 13]. This is due to the photo-corrosion stability and smaller bandgaps (3.2 eV, 2.7 eV, and 1.7 eV for BiOCl, BiOBr, and BiOI, respectively) [14-17].

Because of the characteristics, including two-dimensional (2D) structures and strong internal static electric fields between the layers, which are highly important to reduce the charge carrier's recombination, bismuth oxychloride (BiOCl) has received much attention during the last decades [18, 19]. However, the photocatalytic activity

* *Corresponding Author Email: mohsenpadervand@gmail.com*

of BiOCl is considerably restricted due to the surface defects (acing as likely centers to facilitate e-h recombination and light absorption ability properties [20-22]. Till now, many methods have been investigated to improve the photocatalytic activity of BiOCl based on the morphological control to reach ultra-thin atomic layers [23, 24], induction of oxygen vacancy [25, 26], surface modification with noble metals [27, 28], and coupling with other photocatalysts such as $CdIn_2S_4$ [29], Bi_2WO_6 [30], Mn_3O_4[31], carbon-based polymeric structures [32, 33], etc. Ma et al. prepared MWCNTs/BiOCl composites via a routine hydrothermal process, which showed excellent ability to degrade organic contaminants compared to pure BiOCl under irradiation [34]. The increased photocatalytic activity was attributed to the controlled recombination rate of the electron-hole pairs due to the presence of MWCNTs in the composites [34]. Recently, Zhang et al. produced g-C_3N_4/BiOCl heterojunction with a two-step hydrothermal calcination method [35]. Heterojunction photocatalysts indicated 8.15 times higher degradation ability for Rhodamine B (RhB) and 6.97 times higher H_2 evolution rate than pristine g-C_3N_4 [35]. Lin et al. fabricated some novel graphene oxide/BiOCl composite films via a spread coating method, which exhibited prior photocatalytic activity of 12.2 times higher than pure BiOCl toward the removing RhB under visible light [36].

Carbon-based photocatalysts can be used to purify the environment, water disinfection, produce value-added chemicals, and produce renewable fuels [37-40]. Carbon quantum dots (CQDs) are a group of spherical carbon materials less than 10 nanometers in diameter. Since the discovery of CQDs in 2004, researchers have considered their unique properties such as low toxicity, reasonable production cost, chemical stability, high biocompatibility, and suitable charge separation [41, 42]. CQDs have become an attractive option in modifying several structures and improving photocatalytic activity due to trapping the photogenerated electrons and up-conversion photoluminescence (UC-PL) [43, 44]. Based on the abovementioned reasons, CQDs have been used in designing several photocatalytic systems, including CQDs/Bi_3O_4Br [14], CQDs/Bi_2WO_6 [45], CQDs/$CoFe_2O_4$ [46], CQDs/$PbTiO_3$ [47], etc. We are also aimed to reach prior photocatalytic performance taking advantage of the specific physicochemical properties of BiOCl and CQDs, which make them suitable candidates to prepare an efficient heterojunction with excellent photoactivity.

Herein, we synthesized a nanocomposite comprising BiOCl modified with CQDs using a facile hydrothermal method. The prepared CQDs/BiOCl photocatalysts were well characterized using a multi-technique approach. The photocatalytic activity was evaluated for degrading the anionic dye Congo red in the aqueous phase. We also discussed the kinetics and possible mechanism of the decomposition process, highlighting the critical role of CQDs in improving the optical behavior of pristine BiOCl.

MATERIALS AND METHODS

BiOCl nanosheets

Bi $(NO_3)_3.5H_2O$, 2 mmol, was dissolved in 0.1 M mannitol solution. The NaCl solution was added under vigorous stirring and sonicating conditions. The obtained suspension was then transferred to an autoclave which was kept at 423 K for 3 h. The white precipitate was collected, washed with distilled water repeatedly, and dried at 313 K overnight.

CQDs preparation

10 mL of PEG 200 was added to 5 mL of distilled water at room temperature. 2 g of glucose was added under vigorous stirring and sonicating for 10 min. The solution was treated in a microwave with 600 watts of power for 5 min. The product was a yellowish viscous solution contains CQDs.

BiOCl/CQDs photocatalyst

0.1 g of the as-prepared BiOCl powder was added to the CQDs solution under vigorous stirring. The suspension was sonicated for 5 min at room temperature and then treated in the microwave for 5 min. After completing the reaction, the black precipitate was collected, washed with ethanol repeatedly, and dried at 313 K overnight.

Photocatalytic tests

All the experiments were conducted in a cylindrical reactor made of quartz. The photocatalyst powder was dispersed in dye solution under stirring under dark for 15 min to reach adsorption-desorption equilibrium. The visible irradiation source, a 160 W OSRAM lamp, was then turned on, and the processes began. The

concentration of the dye compound solutions was directly determined using a UV spectrophotometer adjusted at dye λ_{max} value, 500 nm. The details to perform the photodegradation tests over the prepared photocatalyst powder are described elsewhere [48].

RESULTS AND DISCUSSION

Characterization of the photocatalysts

XRD

The Crystalline phase of the photocatalyst was explored by XRD analysis, as shown in Fig. 1. The diffraction peaks are all sharp and strong, which shows high crystallization of the photocatalytic structure. Pure BiOCl shows characteristic peaks attributed to the tetragonal phase of BiOCl (PDF#73–2060). The diffraction patterns indicate similarity between pure BiOCl sample and CQDs/BiOCl. Thus, CQDs does not alter the crystal structure of BiOCl, which may be due to the high dispersion, low intrinsic crystallization, and low loaded amount of CQDs [44]. Besides, an insignificant amount of other impurity phases is detected in the CQDs/BiOCl sample, which could be related to the formation of Bi_2O_3.

FTIR

Fig. 2 shows the FTIR spectra of BiOCl and CQD/BiOCl photocatalysts implying the presence of many significant functional groups. Both spectra show sharp bands at 519 cm^{-1} and 527 cm^{-1} which can be attributed to the Bi-O stretches vibrations [18, 26]. The peak at 1070 cm^{-1} corresponds to C-O stretching vibrations of the CQDs [49]. The peaks at 2852 and 2923 cm^{-1} are related to $–CH_2$ groups, originating from the surfactant residues used during BiOCl nanosheets preparation [18, 50]. The observable peak at 1381 cm^{-1} could be ascribed to nitrate ions of bismuth precursor [51]. The peak around 3100−3600 cm^{-1} and 1637 cm^{-1} are assigned to the stretching mode of the hydroxyl groups [52]. From the obtained results, the O-H band intensity in CQDs/BiOCl is considerably weakened compared to BiOCl. Therefore, the presence of bismuth and carbon functional groups in the final product is confirmed.

DRS

The optical properties of the photocatalysts were studied by diffuse reflectance spectroscopy (DRS). Fig. 3 shows the DRS spectra of BiOCl and CQDs/BiOCl photocatalyst. Although BiOCl doesn't indicate significant absorption in the visible light region, CQDs-modified BiOCl offers broad absorption in the sunlight spectrum. This is probably because of the particle size distribution and the up-conversion effect of CQDs, which affect pristine BiOCl nanosheets. Based on the Tauc method to find the bandgap, plotting $(Ahv)^{1/2}$ and $(Ahv)^2$ versus hv, the gap energy (Eg) of pure BiOCl and CQDs/BiOCl were estimated to be 3.16 eV and 1.15 eV, respectively [53, 54].

TGA

The thermal stability of the prepared photocatalysts was explored by TGA analysis.

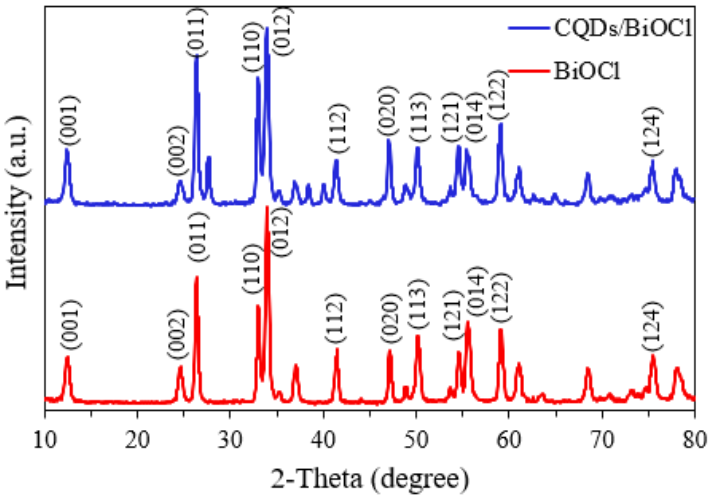

Fig. 1. XRD patterns of pure BiOCl and BiOCl/CQD photocatalysts.

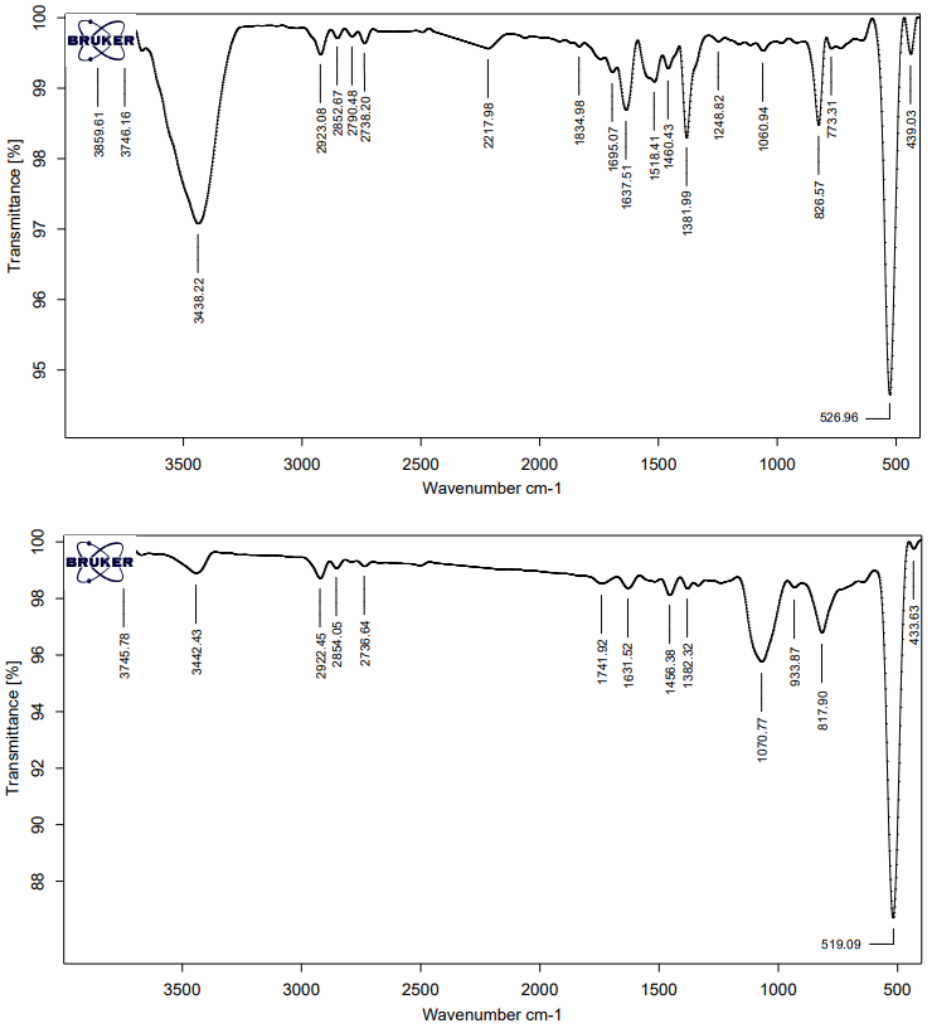

Fig. 2. FT-IR plots of pure BiOCl (up) and BiOCl/CQD (down).

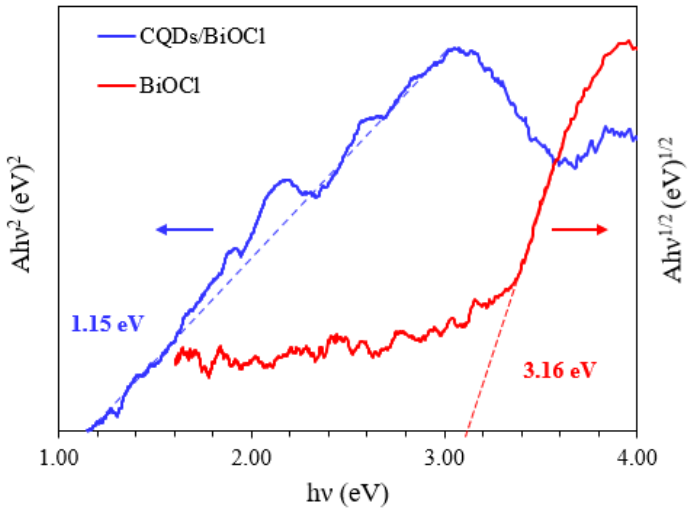

Fig. 3. The results of UV–vis diffuse reflectance analysis.

According to Fig. 4, the weight loss after the total heating treatment was 11.3% and 16.6% for BiOCl and CQDs/BiOCl, respectively. Weight loss at lower than 490 °C is most possibly due to removing water from the structure and other impurities [54]. Weight loss with a steep slope above 600 °C is due to the collapse of the graphitic structure and the cleavage of the functional group of CQDs, as is obvious in the curves [42]. In opposition, BiOCl decomposes to BiO and gaseous Cl_2 at 610 °C and begins to lose more weight at higher temperatures, meaning that BiOCl transformed to Bi_2O_3 [55, 56]. The results of this analysis demonstrate the effect of CQDs on improving the thermal properties of the photocatalyst leading to introduce an efficient heterojunction for the removal of wastewaters.

SEM

The morphology of the prepared 2D sheet-like photocatalysts, including BiOCl and CQDs/BiOCl, is investigated by SEM analysis (Fig. 5 and Fig. 6). The mean particle size is below 200 nm. Also, the sheet thickness in both pure BiOCl and CQDs/BiOCl structures is less than 100 nm. From the images, the CQD/BiOCl sheets are thicker than BiOCl, resulting in the increase of the specific surface area after modifying BiOCl with CQDs. The EDS mapping results for BiOCl and CQDs/BiOCl nanostructures are shown in Fig. 5 and Fig. 6, which prove the purity of the synthesized materials in terms of elemental distribution percentage. The EDS mapping images demonstrate the uniform distribution of CQDs on the surface of BiOCl nanosheets, which is of great importance toward reaching more efficient photocatalytic performance.

BET and BJH

The porosity of the pure BiOCl and CQDs/BiOCl nanostructures was investigated using N_2 adsorption/desorption isotherms (BET analysis, Fig. 7). According to the summary of analysis results shown in Table 1, after modifying BiOCl with CQDs, the specific surface area was remarkably increased. Also, the pore volume and pore size distribution decreased, which could be due to the filling of some mesoporous pores with CQDs. Therefore, implying that the presence of CQDs segments in the final structure. Based on the BJH analysis, the Maximum pore diameter is 39.3 nm and 1.3 nm for BiOCl, CQD/BiOCl, respectively. Hence, by adding CQDs to mesoporous BiOCl, the final structure is classified as micropores material.

Photocatalytic degradation of Congo red solution

Congo red solutions were degraded over the prepared photocatalysts under visible light at room temperature, and the results are shown in Fig. 8 a-c. The CQDs enhanced the photocatalytic activity of BiOCl significantly, as was expected from the DRS analysis results, which confirmed the improvement of light-harvesting properties. From Fig. 8, the concentration of Congo red didn't decrease remarkably in the absence of an illumination source at the same time, meaning that an insignificant amount of removal is due to

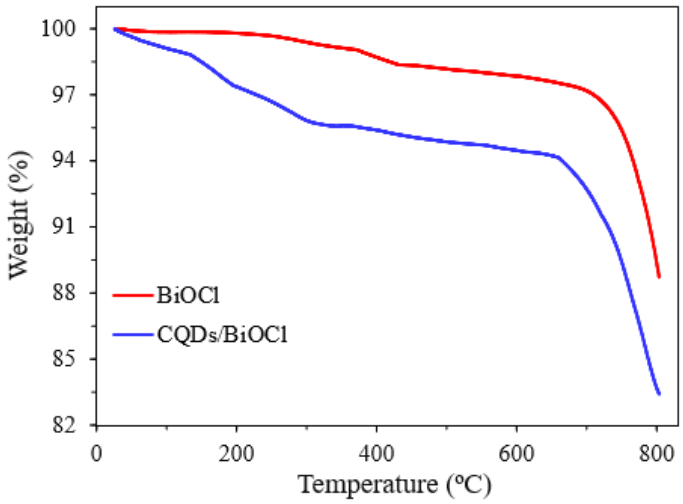

Fig. 4. TGA weight loss curves of pure BiOCl and CQDs/BiOCl.

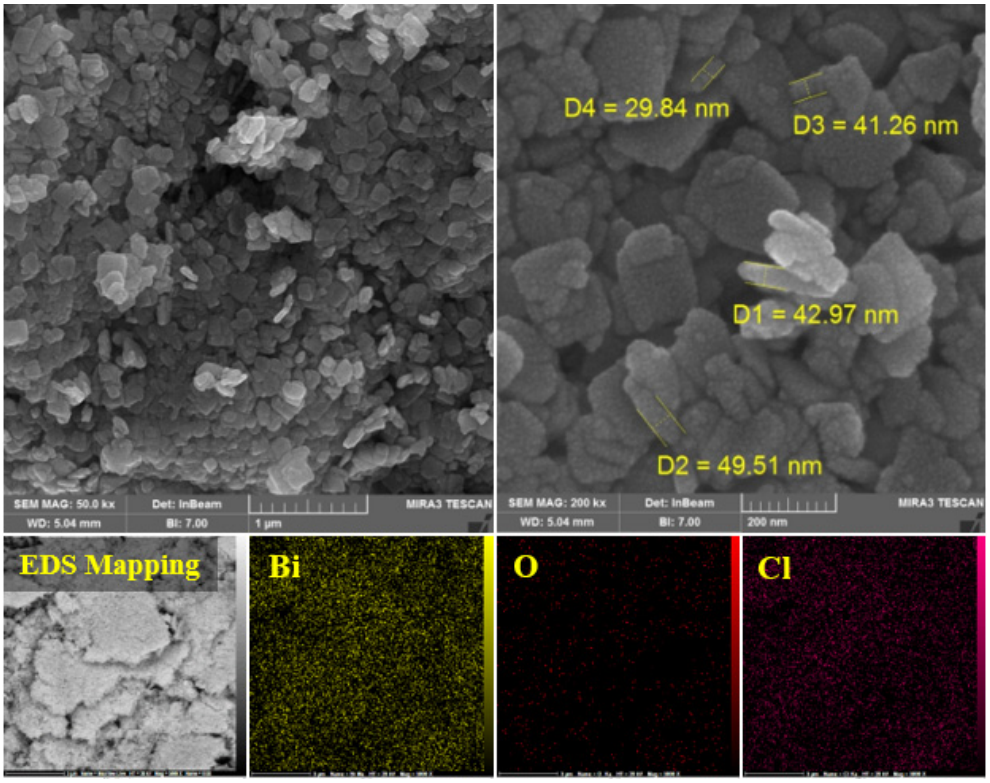

Fig. 5. SEM images of the pure BiOCl; and EDS mapping images of the Bi, O, and Cl.

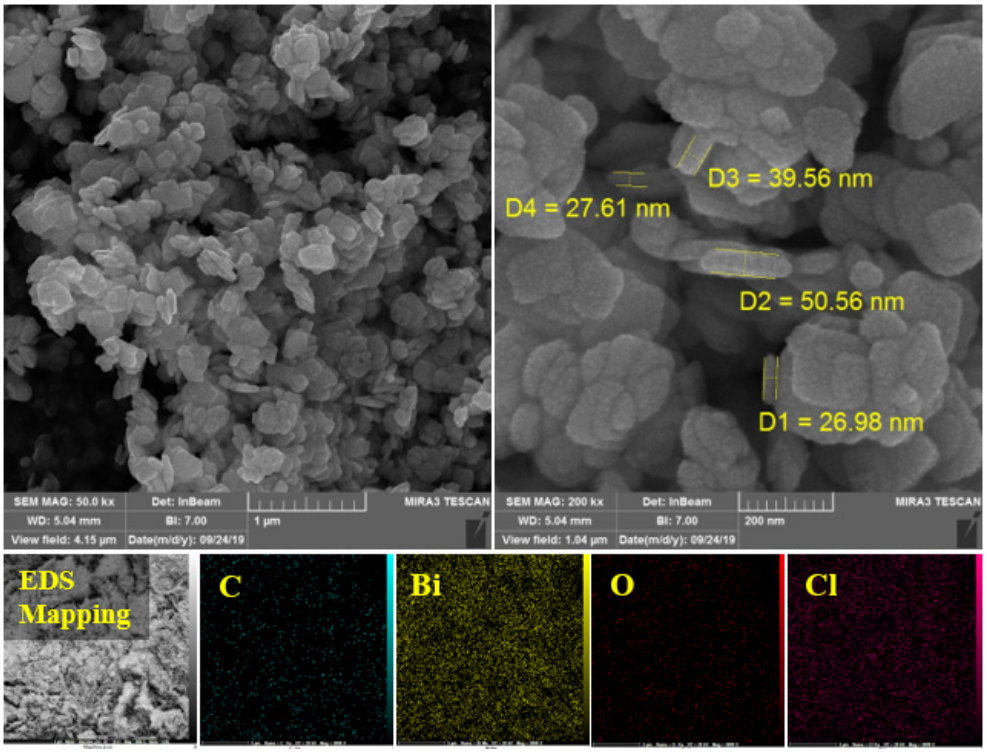

Fig. 6. SEM images of the CQDs/BiOCl; and EDS mapping images of the Bi, O, Cl, and C.

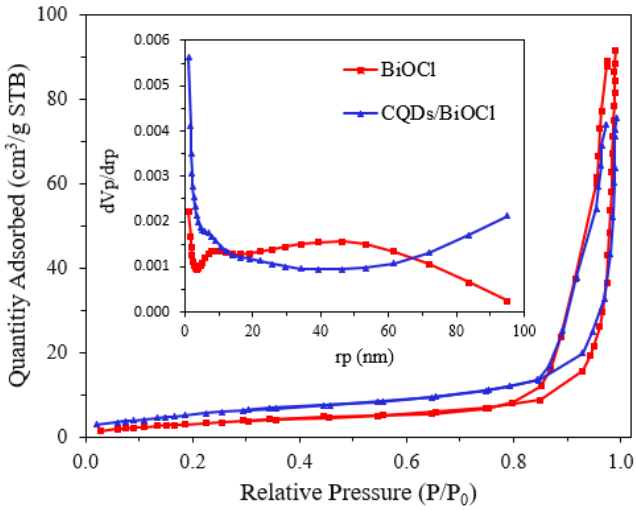

Fig. 7. N_2 adsorption-desorption isotherms and (the inset) corresponding BJH pore-size distribution curves of the Pure BiOCl, CQDs/BiOCl structures.

Table 1. Summarized surface properties of pristine BiOCl and BiOCl/CQDs photocatalysts.

	BET	BJH	
Photocatalyst	Surface area ($m^2 g^{-1}$)	Pore volume ($cm^3 g^{-1}$)	Pore size (nm)
BiOCl	12.3	0.14	39.3
BiOCl/CQDs	19.7	0.11	1.2

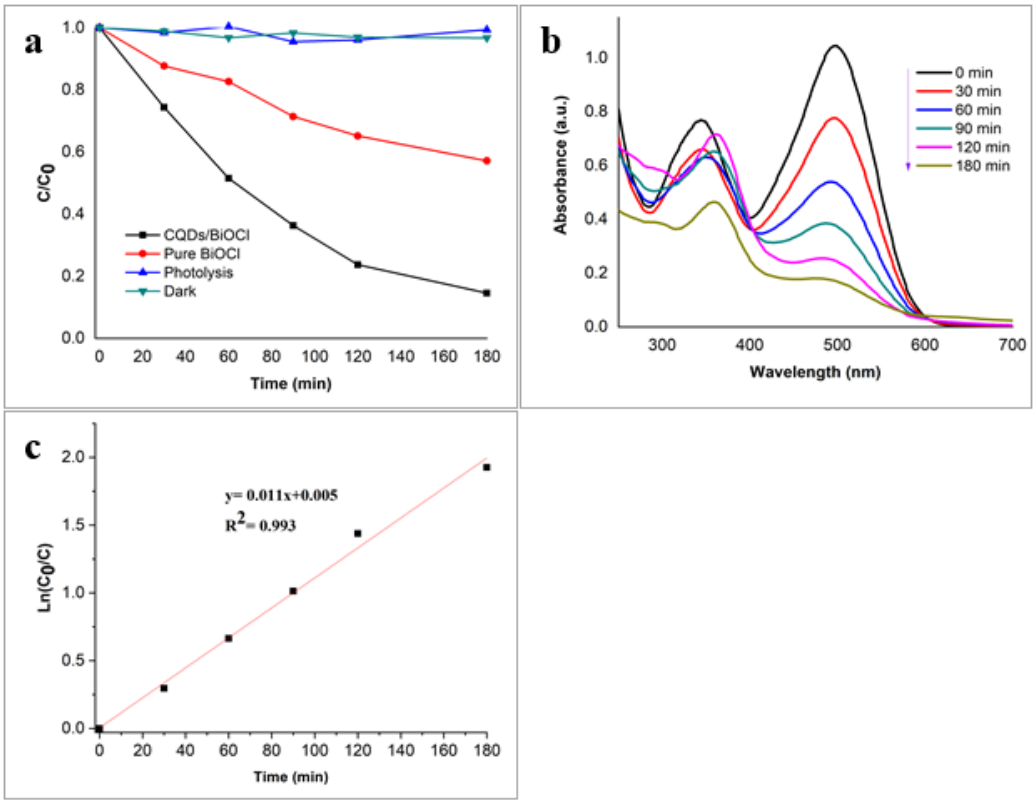

Fig. 8. The results of congo red removal under different conditions (a), UV-vis spectra of the dye compound solutions during the photocatalytic treatment (b) and kinetic fitting of the photoreaction (c).

adsorption on the surface of the photocatalyst. Moreover, the photoreaction obeyed first-order kinetics with the rate constant of 0.011 min^{-1}, deduced from plotting Ln (A_0/A) versus reaction time. The results of the photolysis experiment, treating the dye solution with just irradiation and without any photocatalyst powder, implied no decrease in dye concentration during 180 min of the reaction time. From the abovementioned statements, the main process that occurred in the reaction vessel was "photocatalytic degradation" over the prepared nanostructures.

To reach the optimum conditions and highest removal efficiency, the photodegradation was explored with different amounts of photocatalyst powder, pH, and various concentrations of Congo red. Catalyst dosage changed from 5 to 40 mg; the results showed that the optimum dosage could be 25 mg which led to the fastest degradation during 3 h of the reaction time, Fig. 9 a. Higher amounts of the photocatalyst powder blurred the medium resulting in a decrease of photon absorption by the photosensitive particles which affects photocatalytic performance adversely. Also, the presence of CQDs on the surface enhanced the chance of aggregation in the aqueous medium, a phenomenon that affects the number of photocatalytic active sites on the surface negatively.

Exploring the effect of dye concentration on the photocatalytic efficiency indicated that the best concentration to reach the fast degradation is 10 ppm, Fig. 9 b. More than 10 ppm of Congo red concentration decreased photodegradation efficiency significantly, which is explainable based on the interference of the excessive number of dye molecules with incident light photons to reach the photocatalyst surface. As a result, photolysis was likely much more than photocatalytic degradation, and removal efficiency reduced. To examine the effect of pH on the reaction efficiency, photodegradation was investigated in three pH values. From the results, Fig. 9 c, the highest efficiency obtained in pH= 6.5 while pH of 2.0 and 10.0 affected the photoreaction adversely. This might be due to the

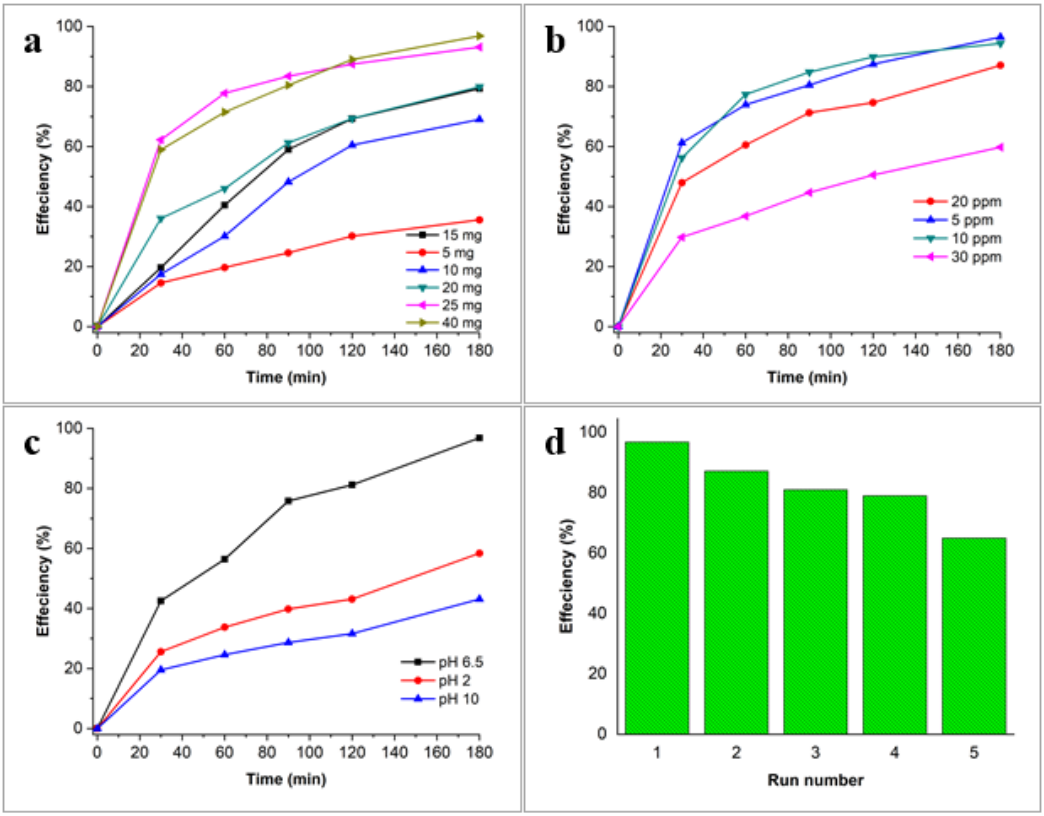

Fig. 9. The effect of catalyst dosage (a), dye concentration (b), and pH (c) on the photocatalytic degradation of congo red and the results of recycling experiments (d).

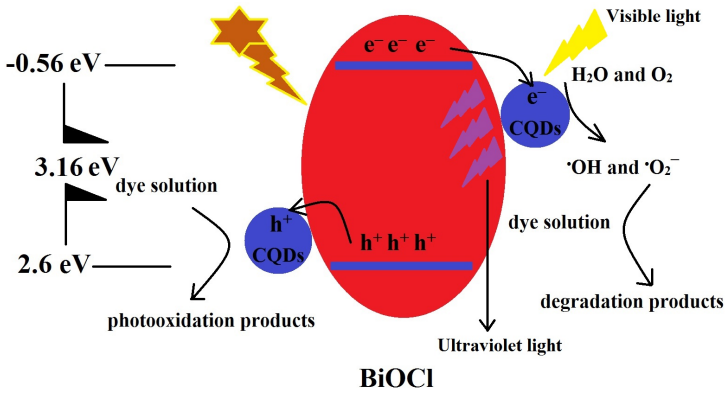

Fig. 10. Schematic demonstration of the photocatalytic performance of CQDs/BiOCl.

chemical structure of Congo red, an anionic dye compound, which could be effectively adsorbed on the surface of the photocatalytic particles in a mildly acidic medium (pH of 6.5). In the alkaline medium, although the hydroxyl ions are expected to enhance the production of OH radicals and facilitate photocatalytic degradation, these negatively-charged species compete with the anionic Congo red molecules for being adsorbed on the surface of the solid particles. As a result, Congo red photocatalytic degradation over CQDs/BiOCl showed the lowest efficiency in pH of 10.0 under visible light.

Recycling experiments were performed to examine if the prepared nanostructure is a promising photocatalyst for practical applications. According to the obtained results, Fig. 9 d, the removal efficiency reduced from 96.8% to 65% after five times repeated use, which is an adverse signal. This considerable decrease in photocatalytic performance might be due to the weak interactions between the nanosheets surface and CQDs or significant corrosion of the sheets surface during the subsequent contacts with a non-neutral aquatic medium that poison the active sites. To overcome such obstacles about the current photocatalyst, insertion of CQDs into platform bulk structure during the formation of BiOCl nanosheets could be an effective procedure.

From a mechanistic point of view, the electrons of the BiOCl valence band are excited to the conduction band after absorbing the light photons, resulting in electron-hole pairs generation on the surface of the suspended particles. According to the reports, the semiconductors with much more negative conduction bands and positive valence bands are suitable for this purpose. They are used as promising photocatalytic material toward removing organic contaminants [57]. While these quantities are favorable about BiOCl (-0.56 and 2.66 eV for its conduction and valence bands, respectively), BiOCl photoactivity is predominantly restricted to the ultraviolet region of the solar light. CQDs can trap the photogenerated electrons of the conduction band and delay electron-hole recombination. This phenomenon enhanced photodegradation efficiency under visible light according to the well-known reactions producing free radicals such as $^{\bullet}OH$ and $^{\bullet}O_2^-$. The photogenerated positive holes can also oxidize dye molecules directly to produce photooxidation products. This is schematically shown in Fig. 10. The photoactivity of pure BiOCl is limited in the visible region due to its large bandgap. However, the prominent role of CQDs causes it to provokes it by emitting ultraviolet photons resulting in the generation of electron-hole pairs [58].

CONCLUSIONS

CQDs decorated BiOCl nanostructures were prepared via a microwave-assisted hydrothermal method. According to DRS analysis, the bandgap was remarkably decreased from 3.16 eV for pure BiOCl to 1.15 eV for CQDs/BiOCl nanostructure. The results of TGA and EDS analyzes confirmed the presence of CQDs on the surface, which were morphologically discussed based on SEM micrographs too. According to the photocatalytic tests, CQDs/BiOCl indicated superior activity than pure BiOCl resulting in a fast decrease of Congo red UV-vis absorption, a pseudo-first-order degradation reaction with the rate constant of 0.011 min^{-1}. Exploring the optimum conditions towards the highest removal efficiency led to

0.04 g, 10 ppm, and 6.5 for the catalyst dosage, dye concentration, and solution pH, respectively. Based on the recycling experiments, the removal efficiency was decreased from 96.8% to 65.0% after five times of repeated use, implying further reconsidering synthesis steps of such photocatalysts to effective insertion of CQDs into the bulk structure.

CONFLICT OF INTEREST

The authors declare that there is no conflict of interests regarding the publication of this manuscript.

REFERENCES

1. Padervand M, Heidarpour H, Bargahi A. A mechanistic study and in-vivo toxicity bioassay on acetamiprid photodegradation over the zeolite supported cerium-based photocatalyst. J Photochem Photobiol A: Chem. 2020;395:112526.
2. Padervand M, Heidarpour H, Goshadehzehn M, Hajiahmadi S. Photocatalytic degradation of 3-methyl-4-nitrophenol over Ag/AgCl-decorated/[MOYI]-coated/ZnO nanostructures: Material characterization, photocatalytic performance, and in-vivo toxicity assessment of the photoproducts. Environmental Technology & Innovation. 2021;21:101212.
3. Salari H. Efficient photocatalytic degradation of environmental pollutant with enhanced photocarrier separation in novel Z-scheme a-MnO_2 nanorod/a-MoO_3 nanocomposites. J Photochem Photobiol A: Chem. 2020;401:112787.
4. Salari H. Kinetics and mechanism of enhanced photocatalytic activity under visible light irradiation using Cr_2O_3/Fe_2O_3 nanostructure derived from bimetallic metal organic framework. Journal of Environmental Chemical Engineering. 2019;7(3):103092.
5. Salari H, Karimi Asl M, Padervand M, Gholami MR. Magnetic metal nanoparticles decorated ionic liquid with excellent antibacterial activity. Journal of Nanostructures. 2020;10(3):613-623.
6. Padervand M, Jalilian E, Majdani R, Goshadezehn M. BiOCl/AgCl-BiOI/AgI quaternary nanocomposite for the efficient photodegradation of organic wastewaters and pathogenic bacteria under visible light. Journal of Water Process Engineering. 2019;29:100789.
7. Padervand M, Rhimi B, Wang C. One-pot synthesis of novel ternary Fe_3N/Fe_2O_3/C_3N_4 photocatalyst for efficient removal of rhodamine B and CO_2 reduction. Journal of Alloys and Compounds. 2021;852:156955.
8. Padervand M, Ghasemi S, Hajiahmadi S, Wang C. $K_4Nb_6O_{17}$/Fe_3N/α-Fe_2O_3/C_3N_4 as an enhanced visible light-driven quaternary photocatalyst for acetamiprid photodegradation, CO_2 reduction, and cancer cells treatment. Applied Surface Science. 2021;544:148939.
9. Padervand M, Gholami K, Salari H, Vosoughi M. Rapid H_2O_2-promoted oxidation of anazolene sodium over the [BMIM]PF=/Pt/γ-Al_2O_3 nanocatalyst. Journal of Nanostructures. 2019;9(3):489-497.
10. Wu S, Li X, Tian Y, Lin Y, Hu YH. Excellent photocatalytic degradation of tetracycline over black anatase-TiO_2 under visible light. Chem Eng J. 2021;406:126747.
11. Basavarajappa PS, Patil SB, Ganganagappa N, Reddy KR, Raghu AV, Reddy CV. Recent progress in metal-doped TiO_2, non-metal doped/codoped TiO_2 and TiO_2 nanostructured hybrids for enhanced photocatalysis. International Journal of Hydrogen Energy. 2020;45(13):7764-7778.
12. Di J, Xia J, Li H, Guo S, Dai S. Bismuth oxyhalide layered materials for energy and environmental applications. Nano Energy. 2017;41:172-192.
13. Ren X, Gao M, Zhang Y, Zhang Z, Cao X, Wang B, et al. Photocatalytic reduction of CO_2 on BiOX : Effect of halogen element type and surface oxygen vacancy mediated mechanism. Applied Catalysis B: Environmental. 2020;274:119063.
14. Huang X, Zhang H, Zhao J, Jiang D, Zhan Q. Carbon quantum dot (CQD)-modified Bi_3O_4Br nanosheets possessing excellent photocatalytic activity under simulated sunlight. Mater Sci Semicond Process. 2021;122:105489.
15. Zhang J, Lei S-l. Interlayer-decoupled BiOX (X=Cl, Br, and I) sheets for photocatalytic water splitting: a computational study. Optoelectronics Letters. 2021;17(1):32-35.
16. Wang S, Wang L, Huang W. Bismuth-based photocatalysts for solar energy conversion. Journal of Materials Chemistry A. 2020;8(46):24307-24352.
17. Cheng H, Huang B, Dai Y. Engineering BiOX (X = Cl, Br, I) nanostructures for highly efficient photocatalytic applications. Nanoscale. 2014;6(4):2009-2026.
18. Wang Z, Chu Z, Dong C, Wang Z, Yao S, Gao H, et al. Ultrathin BiOX (X = Cl, Br, I) Nanosheets with Exposed {001} Facets for Photocatalysis. ACS Applied Nano Materials. 2020;3(2):1981-1991.
19. Cui D, Xu K, Dong X, Lv D, Dong F, Hao W, et al. Controlled hydrogenation into defective interlayer bismuth oxychloride via vacancy engineering. Communications Chemistry. 2020;3(1):1-8.
20. Jiang R, Lu G, Yan Z, Wu D, Zhou R, Bao X. Insights into a CQD-$SnNb_2O_6$/BiOCl Z-scheme system for the degradation of benzocaine: Influence factors, intermediate toxicity and photocatalytic mechanism. Chem Eng J. 2019;374:79-90.
21. Di J, Xia J, Ji M, Wang B, Yin S, Zhang Q, et al. Carbon Quantum Dots Modified BiOCl Ultrathin Nanosheets with Enhanced Molecular Oxygen Activation Ability for Broad Spectrum Photocatalytic Properties and Mechanism Insight. ACS Appl Mater Interfaces. 2015;7(36):20111-20123.
22. Jiang R, Wu D, Lu G, Yan Z, Liu J, Zhou R, et al. Fabrication of Fe3O4 quantum dots modified BiOCl/$BiVO_4$ p-n heterojunction to enhance photocatalytic activity for removing broad-spectrum antibiotics under visible light. Journal of the Taiwan Institute of Chemical Engineers. 2019;96:681-690.
23. Zhang L, Niu CG, Zhao XF, Liang C, Guo H, Zeng GM. Ultrathin BiOCl Single-Crystalline Nanosheets with Large Reactive Facets Area and High Electron Mobility Efficiency: A Superior Candidate for High-Performance Dye Self-Photosensitization Photocatalytic Fuel Cell. ACS Appl Mater Interfaces. 2018;10(46):39723-39734.
24. Jiang J, Zhao K, Xiao X, Zhang L. Synthesis and facet-dependent photoreactivity of BiOCl single-crystalline nanosheets. J Am Chem Soc. 2012;134(10):4473-4476.
25. Li H, Qin F, Yang Z, Cui X, Wang J, Zhang L. New Reaction Pathway Induced by Plasmon for Selective Benzyl Alcohol

Oxidation on BiOCl Possessing Oxygen Vacancies. J Am Chem Soc. 2017;139(9):3513-3521.
26. Wang Q, Wang W, Zhong L, Liu D, Cao X, Cui F. Oxygen vacancy-rich 2D/2D BiOCl-g-C_3N_4 ultrathin heterostructure nanosheets for enhanced visible-light-driven photocatalytic activity in environmental remediation. Applied Catalysis B: Environmental. 2018;220:290-302.
27. Lin H, Ding L, Pei Z, Zhou Y, Long J, Deng W, et al. Au deposited BiOCl with different facets: On determination of the facet-induced transfer preference of charge carriers and the different plasmonic activity. Applied Catalysis B: Environmental. 2014;160-161:98-105.
28. Yu H, Cao C, Wang X, Yu J. Ag-Modified BiOCl Single-Crystal Nanosheets: Dependence of Photocatalytic Performance on the Region-Selective Deposition of Ag Nanoparticles. The Journal of Physical Chemistry C. 2017;121(24):13191-13201.
29. Xiao Y, Peng Z, Zhang S, Jiang Y, Jing X, Yang X, et al. Z-scheme $CdIn_2S_4$/BiOCl nanosheet face-to-face heterostructure: in-situ synthesis and enhanced interfacial charge transfer for high-efficient photocatalytic performance. JMatS. 2019;54(13):9573-9590.
30. Tahmasebi N, Maleki Z, Farahnak P. Enhanced photocatalytic activities of Bi_2WO_6/BiOCl composite synthesized by one-step hydrothermal method with the assistance of HCl. Mater Sci Semicond Process. 2019;89:32-40.
31. Shen T, Shi X, Guo J, Li J, Yuan S. Photocatalytic removal of NO by light-driven Mn_3O_4/BiOCl heterojunction photocatalyst: Optimization and mechanism. Chem Eng J. 2021;408:128014.
32. Sun Y, Qi X, Li R, Xie Y, Tang Q, Ren B. Hydrothermal synthesis of 2D/2D BiOCl/g-C_3N_4 Z-scheme: For TC degradation and antimicrobial activity evaluation. Optical Materials. 2020;108:110170.
33. Wang Q, Hui J, Li J, Cai Y, Yin S, Wang F, et al. Photodegradation of methyl orange with PANI-modified BiOCl photocatalyst under visible light irradiation. Applied Surface Science. 2013;283:577-583.
34. Ma D, Zhong J, Li J, Burda C, Duan R. Preparation and photocatalytic performance of MWCNTs/BiOCl: Evidence for the superoxide radical participation in the degradation mechanism of phenol. Applied Surface Science. 2019;480:395-403.
35. Zhang R, Niu S, Xiang J, Zheng J, Jiang Z, Guo C. Band-potential fluctuation in C_3N_4/BiOCl hetero-junction for boosting photo-catalytic activity. Sep Purif Technol. 2021;261:118258.
36. Lin W, Yu X, Zhu Y, Zhang Y. Graphene Oxide/BiOCl Nanocomposite Films as Efficient Visible Light Photocatalysts. Front Chem. 2018;6:274.
37. Asadzadeh-Khaneghah S, Habibi-Yangjeh A. g-C3N4/carbon dot-based nanocomposites serve as efficacious photocatalysts for environmental purification and energy generation: A review. Journal of Cleaner Production. 2020:124319.
38. Akhundi A, Badiei A, Ziarani GM, Habibi-Yangjeh A, Muñoz-Batista MJ, Luque R. Graphitic carbon nitride-based photocatalysts: toward efficient organic transformation for value-added chemicals production. Molecular Catalysis. 2020;488:110902.
39. Akhundi A, Habibi-Yangjeh A, Abitorabi M, Rahim Pouran S. Review on photocatalytic conversion of carbon dioxide to value-added compounds and renewable fuels by graphitic carbon nitride-based photocatalysts. CarRv. 2019;61(4):595-628.
40. Habibi-Yangjeh A, Asadzadeh-Khaneghah S, Feizpoor S, Rouhi A. Review on heterogeneous photocatalytic disinfection of waterborne, airborne, and foodborne viruses: Can we win against pathogenic viruses? Journal of Colloid and Interface Science. 2020.
41. Molaei MJ. The optical properties and solar energy conversion applications of carbon quantum dots: A review. SoEn. 2020;196:549-566.
42. Abd Rani U, Ng LY, Ng CY, Mahmoudi E. A review of carbon quantum dots and their applications in wastewater treatment. Advances in colloid and interface science. 2020;278:102124.
43. Jiang R, Wu D, Lu G, Yan Z, Liu J. Modified 2D-2D $ZnIn_2S_4$/BiOCl van der Waals heterojunctions with CQDs: Accelerated charge transfer and enhanced photocatalytic activity under vis- and NIR-light. Chemosphere. 2019;227:82-92.
44. Kong XY, Tan WL, Ng B-J, Chai S-P, Mohamed AR. Harnessing Vis–NIR broad spectrum for photocatalytic CO_2 reduction over carbon quantum dots-decorated ultrathin Bi2WO6 nanosheets. Nano Research. 2017;10(5):1720-1731.
45. Liu Y, Zhu C, Sun J, Ge Y, Song F, Xu Q. In situ assembly of CQDs/Bi_2WO_6 for highly efficient photocatalytic degradation of VOCs under visible light. New Journal of Chemistry. 2020;44(8):3455-3462.
46. Ahmadian-Fard-Fini S, Salavati-Niasari M, Safardoust-Hojaghan H. Hydrothermal green synthesis and photocatalytic activity of magnetic $CoFe_2O_4$–carbon quantum dots nanocomposite by turmeric precursor. Journal of Materials Science: Materials in Electronics. 2017;28(21):16205-16214.
47. Kooshki H, Sobhani-Nasab A, Eghbali-Arani M, Ahmadi F, Ameri V, Rahimi-Nasrabadi M. Eco-friendly synthesis of $PbTiO_3$ nanoparticles and $PbTiO_3$/carbon quantum dots binary nano-hybrids for enhanced photocatalytic performance under visible light. Sep Purif Technol. 2019;211:873-881.
48. Padervand M, Lammel G, Bargahi A, Mohammad-Shiri H. Photochemical degradation of the environmental pollutants over the worm-like Nd_2CuO_4-Nd_2O_3 nanostructures. Nano-Structures & Nano-Objects. 2019;18:100258.
49. Zhang Q, Zhang X, Bao L, Wu Y, Jiang L, Zheng Y, et al. The Application of Green-Synthesis-Derived Carbon Quantum Dots to Bioimaging and the Analysis of Mercury(II). J Anal Methods Chem. 2019;2019:8183134.
50. Sánchez-Rodríguez D, Méndez Medrano MG, Remita H, Escobar-Barrios V. Photocatalytic properties of BiOCl-TiO_2 composites for phenol photodegradation. Journal of Environmental Chemical Engineering. 2018;6(2):1601-1612.
51. Chen Q, Feng NB, Huang XH, Yao Y, Jin YR, Pan W, et al. Humidity-Sensing Properties of a BiOCl-Coated Quartz Crystal Microbalance. ACS Omega. 2020;5(30):18818-18825.
52. Zhang L, Wang W, Jiang D, Gao E, Sun S. Photoreduction of CO_2 on BiOCl nanoplates with the assistance of photoinduced oxygen vacancies. Nano Research. 2014;8(3):821-831.
53. Li Q, Guan Z, Wu D, Zhao X, Bao S, Tian B, et al. Z-Scheme BiOCl-Au-CdS Heterostructure with Enhanced Sunlight-

Driven Photocatalytic Activity in Degrading Water Dyes and Antibiotics. ACS Sustainable Chemistry & Engineering. 2017;5(8):6958-6968.
54. Deng F, Lu X, Zhong F, Pei X, Luo X, Luo S, et al. Fabrication of 2D sheet-like BiOCl/carbon quantum dot hybrids via a template-free coprecipitation method and their tunable visible-light photocatalytic activities derived from different size distributions of carbon quantum dots. Nanotechnology. 2016;27(6):065701.
55. Mera AC, Rodríguez CA, Pizarro-Castillo L, Meléndrez MF, Valdés H. Effect of temperature and reaction time during solvothermal synthesis of BiOCl on microspheres formation: implications in the photocatalytic oxidation of gallic acid under simulated solar radiation. Journal of Sol-Gel Science and Technology. 2020;95(1):146-156.
56. Rivera EJ, Tran LA, Hernandez-Rivera M, Yoon D, Mikos AG, Rusakova IA, et al. Bismuth@US-tubes as a Potential Contrast Agent for X-ray Imaging Applications. J Mater Chem B. 2013;1(37):4792-4800.
57. Qu Z, Wang J, Tang J, Shu X, Liu X, Zhang Z, et al. Carbon quantum dots/$KNbO_3$ hybrid composites with enhanced visible-light driven photocatalytic activity toward dye waste-water degradation and hydrogen production. Molecular Catalysis. 2018;445:1-11.
58. Pirsaheb M, Asadi A, Sillanpää M, Farhadian N. Application of carbon quantum dots to increase the activity of conventional photocatalysts: a systematic review. J Mol Liq. 2018;271:857-871.